# Aerodynamic Performance Investigations of Savonius Twin-rotor Wind Turbines

M. Tata[1†], A. Bekhti[1], M. Maizi[1], N. O. Cherifi[2], A. Tamoum[2], D. Hamane[1], A. Boudis[1], M. Debbache[1] and O. Guerri[1]

*[1] Center for Renewable Energies Development, CDER, BP 62 Road of the Observatory, Bouzareah, 16340, Algiers, Algeria*
*[2] Mohamed Bougara University, Technology Faculty, Mechanical Engineering Department, Boumerdes, Algeria*

*†Corresponding Author Email: m.tata@cder.dz*

## ABSTRACT

The aim of this study is to evaluate the aerodynamic efficiency of a Savonius vertical-axis wind turbine. The approach used relies on resolving the Unsteady Reynolds Averaged Navier-Stokes equations (URANS), the turbulence being modeled by the k-ω SST model. The flow around the wind turbine is simulated using the arbitrary sliding interfaces technique. First, the study investigates the impact of blade shape on wind turbine efficiency by examining seven Savonius rotors constructed with distinct blade configurations. The results indicate that the highest aerodynamic performance is provided by the rotor with the elliptical blades, with a notable increase in the power coefficient of about 80% in comparison to the classic semi-circular profile. To further enhance the efficiency of the Savonius wind turbine, a twin-rotor configuration using the elliptical blades was studied. The results indicate a further enhancement in the power coefficient, reaching 110% compared to a single rotor with semicircular blades.

## 1. INTRODUCTION

Savonius rotor is a drag-driven vertical axis wind turbine (VAWT). Compared to horizontal axis wind turbines, the efficiency is lower for this kind of wind turbines, and the yield is low, but its construction is simple and requires few means. However, it is mostly silent and has the ability to produce power at low wind speeds. Therefore, it is appropriate for use in urban environments.

The conventional Savonius rotor was pioneered by Johannes (1929), made up of two off-centered semi-circular. A profile composed of linear segment and a curved arc, the Bach profile, was also used instead of semi-circular blades (Bach, 1931). Subsequently, various blade shapes were suggested. The main geometrical parameters of the Savonius rotors are represented in Fig. 1 where (D) and (H) are the diameter and the height of the rotor respectively, (d) is the blade chord, and (e) is the width of the gap between the blades.

Savonius rotors have been the subject of many studies to assess the impacts of the several geometric parameters that affect its aerodynamic performances such as the aspect ratio H/D, the overlap ratio, the blade number, the number of rotor stages, and the blade shape. The

interaction of Savonius rotors in wind farms has also been investigated.

Regarding single rotors, (Saha et al., 2008) carried out wind tunnel experiments to evaluate the performances of different Savonius rotors built with semicircular and twisted blades. They considered single-, two- and three-stage rotors, two and three-blade rotors, and valve-aided rotors. The main observations they reported were that the ideal number of blades is two, regardless of the number of rotor stages, rotors with twisted blades had good performance compared to rotors with semi-circular blades, two-stage rotors had the best power coefficient, and the three-bladed valve-assisted Savonius rotor outperforms the conventional three-bladed rotor regarding its power coefficient. Mohamed et al. (2011) carried out numerical computations to improve the blade profile of Savonius rotors. They applied a fully coupled optimization procedure based on the CFD code Ansys-Fluent and their optimization algorithms (OPAL). Taking into account a rotor with an obstacle plate positioned for optimal performance identified in a previous study, the optimal blade shape led to a power coefficient increase of 38.9% at the tip speed ratio (TSR) equal to 0.7, and an overall gain of about 30% over for the entire operating range.

| Nomenclature | | | |
|---|---|---|---|
| $A$ | rotor swept area | TSR | Tip Speed Ratio |
| $C_P$ | power coefficient | $u_i$ | velocity components |
| d | blade chord | $V$ | free stream velocity |
| D | rotor diameter | $x_i$ | coordinate components |
| e | gap | $y_p$ | first node near the rotor wall |
| $e_P$ | blade thickness | **Greek letters** | |
| $F_1$, $F_2$ | blending functions | $\alpha$, $\beta$ | turbulent constants |
| H | rotor height | $\varepsilon$ | dissipation rate |
| K | turbulent kinetic energy | $\nu$ | kinematic viscosity |
| $p$ | pressure | $\nu_T$ | turbulent kinematic viscosity |
| $P_{available}$ | available power in the wind | $\rho$ | air density |
| $P_m$ | generated power | $\omega$ | specific dissipation rate |
| $R$ | rotor radius | $\Omega$ | rotational speed |
| $T$ | torque | $\Omega_f$ | fluid domain |

Akwa et al. (2012) presented a review of a few studies on the impact of the geometric parameters, Reynolds number, turbulence scales and stators that influences the efficiency of a Savonius wind rotor. The researchers have observed a consensus in the literature regarding the ideal endplate size for Savonius wind rotors, aspect ratio value of around 2, zero bucket spacing for semi-circular profile Savonius rotors, and the reduction in the power produced when the blades number is greater than 2. However, there was no consensus on other characteristics such as the optimal blade overlap and the mean power coefficient. In their extensive review of numerical studies applied to Savonius rotors, Roy and Saha (2013) also observed that while the influencing parameters were optimized to some extent, they have not been precisely optimized to an accurate value. Zhou and Rempfer (2013) carried out numerical simulations applied to two Savonius rotors, one built with a semicircular shape and the second with a Bach profile. They demonstrated that the power coefficient of the rotors built with the Bach profile is higher than with a conventional blade. Kacprzak et al. (2013) performed numerical investigations on the fluid flow patterns through traditional, Bach-type and elliptical blade Savonius rotors. Among their main results, they noticed that the three rotors attained maximum power coefficient at TSR=0.8, the Bach-type rotor performance was the highest, and that for TSR values between 0.2 and 0.4 the Elliptical Savonius rotor performed better. Banerjee et al. (2014) applied CFD computations to assess the efficiency of rotors built with elliptical blades. They showed that a 10.7% of enhancement in power coefficient was achieved with the elliptical profile when compared to the traditional semi-circular profile. Driss et al. (2014) conducted both experimental and numerical studies into the turbulent flow through a small Savonius wind turbine with incurved rotor profile. They noticed that the fluid circulation of this rotor was improved compared to a circular Savonius rotor. Likewise, Diaz et al. (2015) used a computational method to examine the impact of the number of rotor stages, the rotor shape, and the blade number. Considering different Savonius rotor configurations, they noticed that rotors with more than two blades recorded lower power output and that helical blade rotors had higher power coefficients. In Roy and Saha (2013), wind tunnel tests have been carried out using a novel turbine blade shape, as well as standard semi-circular, semi-elliptic, Benesh, and Bach

blades for comparison. Alom et al. (2016) modified the shape of an elliptical blade to optimize the performance of elliptical-bladed Savonius rotors. In their critique of Savonius rotors' design parameters, Al-kayiem et al. (2016) also concluded that the geometrical characteristics of this specific kind of wind turbine should be optimized and that improving the shape of the blades could also increase their performance. Continuing these investigations, Bhayo and Al-kayiem (2017) conducted an open wind flow investigation involving seven variants of Savonius models with various blade designs, blades number, and number of stages. Chen et al. (2018) performed a thorough summarization and in-depth discussion of the performance and distinctive features exhibited by various blade profiles. They mainly reported that the well-designed Bach rotor and helical rotor demonstrated superior performance compared to the traditional Savonius rotor. Conversely, the $C_{P(MAX)}$ of the twisted rotors was not notably higher than the $C_{P(MAX)}$ of the Savonius rotors. El-Askary et al. (2018) conducted numerical and experimental investigations to assess the effectiveness of a modified twisted Savonius rotor. According to their findings, the optimal twist angle for the modified rotor was determined to be 45°. Ebrahimpour et al. (2019) conducted a study to examine the impact of the overlap ratio on the wind turbine performance. For this purpose, they performed two-dimensional numerical simulations using URANS equations and the sliding mesh method. Considering a classic Savonius rotor, they showed that better performances are achieved when the overlap ratio is equal to 0.15. Another extensive review of the impact of geometric parameters and rotor blade profiles and shapes was presented by (Alom and Saha 2019a). Research applying optimization techniques to the design of blade profiles was cited. Thereafter in Alom and Saha (2019b) performed experimental and 2D simulations to explore the impact of different blade shapes on the effectiveness of a Savonius wind turbine. They considered four different blade profiles for the Savonius wind turbine: semicircular, Benesh, modified Bach and elliptical profiles. For each profile, they maintained a constant overall rotor diameter to enable a fair comparison of their respective performances and characteristics. They found that the highest power coefficient is provided by the elliptical profile. Ashwindran et al. (2020) performed numerical computations to assess the efficiency of six

Savonius turbines built with different profiles. They showed that the rotor built with the Sivasegaram profile, which is a composite blade shape formed by combining a small and a large curvature, exhibited superior moment coefficient than the traditional semicircular rotor, with an improvement of 7.2% of moment coefficient at TSR = 0.59. To further enhance the effectiveness of Savonius rotors, Shashikumar et al. (2021) carried out experimental investigations and three-dimensional computations to compare five V-shaped rotors. The V-angle of the profiles was maintained fixed to 90°, while the length of V-edge was varied. Their study targeted the use of hydropower. Anupam et al. (2021) conducted a review of multiple studies focused on enhancing the effectiveness of the Savonius rotor. They showed that the elliptical profile produces the maximum power coefficient of 0.34. Conversely, a two-stage, two-blade Savonius rotor with an elliptical shape was investigated by Patel et al. (2023). They utilized the SST k-ω turbulence model to perform their simulations. They discovered that the highest power coefficient achieved by the two-stage rotor was 0.21, which represented a 39.4% improvement over the single-stage rotor.

Concerning Savonius rotors in wind farm arrangements, it was reported that interactions between Savonius turbines in a cluster have the potential to improve the power generation of individual rotors. In this context, Sun et al. (2021) conducted numerical simulations of two standard Savonius rotors arranged in parallel and oblique configurations. They considered also an arrangement of three Savonius rotors. Their conclusion stated that the interaction between the Savonius rotors could exhibit either positive or negative effects, depending on factors such as the relative direction of rotational motion, the spacing between the wind turbines, and the angular difference in the positions of the rotors. Shaheen et al. (2015) carried out also numerical simulations to study groups of two and three Savonius turbines built with semicircular blades. In scenarios involving of two parallel rotors, the highest performance was achieved when the spacing between the rotors equaled 0.2 times the diameter of the rotor. Regarding oblique arrangements, an angle of 60° proved to be the most effective in avoiding the wake of the upstream rotor. Regarding the three rotors cluster of Savonius turbines, the authors found that the configuration with two rotors positioned upstream and one rotor downstream demonstrated the highest performance, the optimal configurations of the two wind turbines in parallel and oblique being applied. Likewise, El-Baz et al. (2016) conducted an evaluation of the efficiency of three Savonius rotors assembled in a triangular configuration. They performed 2D numerical computations based on the implementation of the Reynolds averaged Navier-Stokes equations and the realizable k-ε turbulence model, with a sliding mesh technique. Findings were obtained for a configuration comprising a single rotor positioned upstream and two rotors situated downstream, with the first rotor rotating counterclockwise and the two downstream rotors rotating clockwise, with all three rotors were observed to rotate with zero phase shifts. They showed that the three rotors had a superior power coefficient than that of a single rotor. The observed performance improvement has been attributed to the beneficial interaction between the rotors, resulting in accelerated flow as it approaches the downstream rotors. This interaction generates higher torque in the rotational direction for each rotor. However, they noticed that if the wind direction changed, the effectiveness of the three wind turbines could be affected by the interference caused by one rotor on the adjacent rotors. They concluded that therefore, a guiding device would be needed to align the three rotors with the wind direction. The interplay among Savonius wind turbines installed in a cluster has also been investigated by Meziane et al. (2019). The latter considered two Savonius turbines in three arrangements, aligned, parallel, and oblique, and three turbines arranged in a triangle. The outcomes of their study demonstrated an increase in the wind turbines' power coefficient installed in the cluster compared to the single Savonius turbine. Etemadeasl et al. (2021) considered two contra-rotating Savonius rotors and performed numerical computations to investigate the impacts of the distance and the position difference in the azimuthal angle between the two rotors. Their study was conducted for two rotors separated by distances ranging from 0 to 1.5 times the diameter of the rotor. They revealed that the aerodynamic effectiveness of the two rotors exhibited improvements compared to the traditional single rotor configuration. The highest power coefficient was attained when the gap between the two rotors equaled one rotor diameter. Conversely, the difference in angular position would have little influence. They expected that increasing the gap between the rotors would lead to pressure and velocity fields surrounding the two rotors resembling those of an isolated Savonius rotor, thus negating the benefit of the interaction between the two rotors. Recently, Hesami et al. (2022) proposed to add a diffuser to two conventional Savonius rotors in a twin arrangement. They applied a numerical approach to investigate the impact of various operational and geometric parameters on the effectiveness of the ducted twin-rotors. They provided a description of the fluid flow phenomena and noticed mainly that the studied system showed the best enhancement in the power coefficient when the rotors rotations were counter-rotating, and when the separation distance was fixed at 0.36 times the diameter of the rotor. The maximum enhancement in power coefficient reached 114% compared to the performance of an isolated turbine. The effectiveness of a Savonius wind turbine with twin turbines rotating in opposite directions was examined by Altan & Gungor (2022). The latter added a triangular plate positioned in the turbines' front and were thus able to achieve an optimal power coefficient of 0.22, which represented a 30% improvement when compared to a traditional system. Savonius wind turbine clusters with two and three rotors and a semicircular profile were considered by Im and Kim (2022). These authors showed that the installation of several turbines did not result in a reduction of wind turbine performance. Instead, it was observed that the power output could be raised by placing the downstream turbine at a distance equal to twice the diameter of the upstream turbine.

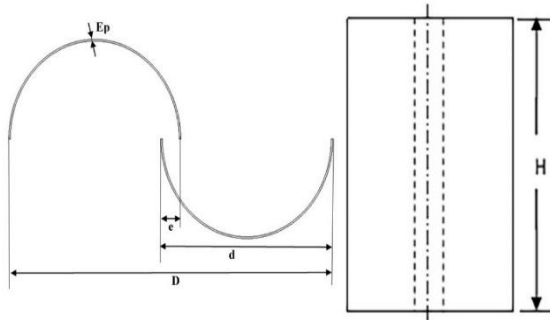In summary, this review shows that blade shape optimization could significantly increase turbine

**Fig. 1 Traditional Savonius rotor**

**Table 1 Rotor dimensions in meters**

| Rotor diameter (D) | 0.2195 |
|---|---|
| blade diameter (d) | 0.115 |
| Blade thickness ($e_p$) | 0.001 |
| Rotor height (H) | 0.2 |
| Gap width (e) | 0.115 |

performance and that a favorable interaction was observed to exist between Savonius turbines in a cluster. Thereby, to enhance the effectiveness of this kind of wind turbine, numerous investigations on the blade shape were carried out. It was shown that the elliptical-bladed rotor can be a strong competitor in the Savonius wind turbine efficiency enhancement. Regarding the effectiveness of the Savonius turbines in clusters, in many studies, conventional Savonius turbines have been considered to investigate the impact of turbine spacing and the direction of rotation of the rotors. The results reported in this review did not show consensus regarding the use of non-conventional blade shape in Savonius turbine clusters.

As noted by Roy and Saha (2013), further numerical research is still needed to more accurately predict rotor performance characteristics and further enhance the effectiveness of the Savonius rotor. Then, in the present study, numerical analyses are first conducted to assess the effectiveness of seven Savonius rotors built with different blade shapes. Then the performances of twin rotors with elliptical blades are computed. To the author's knowledge, in studies applied to twin rotors, only the traditional semi-circular blade rotors were considered (Fig. 1). Less interest has been shown in the impact of the blade profile on the effectiveness of twin-rotor Savonius, whereas the blade shape is an essential design parameter that has a significant influence on the effectiveness of Savonius rotors. Hence, the primary objective of this study is to evaluate the impact of the blade shape on the aerodynamic effectiveness of the Savonius twin-rotor wind turbine. These calculations are performed for a Savonius rotor whose main dimensions are summarized in Table 1. In order to compare the results of these simulations with information from the literature, the dimensions chosen for the rotor are similar to those of the rotor used by Dobrev and Massouh (2011) in their experimental investigations.

## 2. MATHEMATICAL MODEL

The assumption is made that the fluid is incompressible and turbulent. The unsteady Reynolds averaged Navier-Stokes (URANS) equations are resolved in a two-dimensional computational domain. The turbulence is modeled by the popular Shear Stress Transport (SST) k-ω model of Menter (1993). The SST k-ω model is a two-equation approach that incorporates the strengths of both the k-ε and k-ω turbulence models. The SST k-ω formulation enables a transition from the k-ω model in proximity to the wall, to the *k-ε* model in the open flow region. This transition help mitigates the sensitivity of the k-ω turbulence model to the turbulence characteristics of the freestream flow. Patel et al. (2023) examined the aerodynamic properties of a 2-stage, 2-blade Savonius rotor. The authors conducted their simulations utilizing the SST k-ω turbulence model. Chan et al. (2018) conducted a numerical investigation aimed at optimizing the design of the Savonius wind turbine in order to enhance its power coefficient. In their simulations, turbulence was also represented by the SST k-ω turbulence model.

### 2.1 Model Equations

Let $\Omega_f \in \mathbb{R}^2$ be the spatial domain occupied by the fluid. The incompressible URANS equations are written as, in tensor notation:

- Continuity equation:

$$\frac{\partial u_i}{\partial x_i} = 0 \tag{1}$$

- Momentum equation:

$$\frac{\partial u_i}{\partial t} + u_j \frac{\partial u_i}{\partial x_j} = -\frac{1}{\rho}\frac{\partial P}{\partial x_i} + \frac{(\mu+\mu_t)}{\rho}\left[\frac{\partial^2 u_i}{\partial x_j \partial x_j}\right] \tag{2}$$

where *t* is the time, $x_i$ is the Cartesian coordinate of a point of $\Omega_f$, $u_i$ is the velocity component in the *i* direction, *p* is the pressure, and *ρ* is the fluid density.

The SST k-ω turbulence model equations write as:

- Turbulent kinetic energy transport *k*:

$$\frac{\partial k}{\partial t} + u_j \frac{\partial k}{\partial x_j} = P_k - \beta^* k\omega + \frac{\partial}{\partial x_j}\left[(\nu + \sigma_k \nu_T)\frac{\partial k}{\partial x_j}\right] \tag{3}$$

- Specific Dissipation rate of turbulent energy ω:

$$\frac{\partial \omega}{\partial t} + u_j \frac{\partial \omega}{\partial x_j} = \alpha S^2 - \beta \omega^2 + \frac{\partial}{\partial x_j}\left[(\nu + \sigma_\omega \nu_T)\frac{\partial \omega}{\partial x_j}\right] +$$
$$2(1 - F_1)\sigma_{\omega 2}\frac{1}{\omega}\frac{\partial k}{\partial x_i}\frac{\partial \omega}{\partial x_i} \tag{4}$$

$\beta^*$, β, $\sigma_k$ and $\sigma_\omega$ are the model constants, whose values are summarized in Table 2, and $F_1$ is the function that allows switching from the k-ω model to the k-ε model:

$$F_1 = \tanh\left\{\left\{\min\left[\max\left(\frac{\sqrt{k}}{\beta^* \omega y}, \frac{500\nu}{y^2 \omega}\right), \frac{4\sigma_{\omega 2}k}{CD_{k\omega}y^2}\right]\right\}^4\right\} \tag{5}$$

$$CD_{k\omega} = \max\left(2\rho\sigma_{\omega 2}\frac{1}{\omega}\frac{\partial k}{\partial x_i}\frac{\partial \omega}{\partial x_i}, 10^{-10}\right) \tag{6}$$

**Table 2 SST k-ω model constants**

| $\beta^*$ | $\beta_1$ | $\beta_2$ | $\sigma_{k1}$ | $\sigma_{k2}$ | $\sigma_{\omega 1}$ | $\sigma_{\omega 2}$ |
|---|---|---|---|---|---|---|
| 0.09 | 0.075 | 0.0828 | 0.85 | 1 | 0.5 | 0.856 |

The kinematic viscosity $\nu_T$ is written as:

$$\nu_T = \frac{a_1 k}{\max(a_1 \omega, SF_2)} \tag{7}$$

$$F_2 = \tanh\left[\left[max\left(\frac{2\sqrt{k}}{\beta^* \omega y}, \frac{500\nu}{y^2 \omega}\right)\right]^2\right] \tag{8}$$

More details regarding this model can be found in (Menter, 1993).

## 2.2 Performance Calculation

Wind turbine performance is commonly described by the torque coefficient $C_T$ and the power coefficient $C_P$. These parameters are expressed by:

$$C_T = \frac{T}{1/2 \cdot \rho \cdot A \cdot V^2 \cdot R} \tag{9}$$

$$C_p = C_T \cdot TSR \tag{10}$$

where $T$, $V$, $R$, and $A$ are respectively, the produced torque, the free stream wind velocity, the rotor radius, the rotor swept area ($A = H \cdot D$), and TSR, which is characterized as the ratio of the rotor tip speed divided by the free stream velocity:

$$TSR = \frac{\Omega \cdot R}{V} \tag{11}$$

The aerodynamic torque is calculated from summing the moment due to pressure forces around the oz direction and the moment due to viscosity forces around the oz direction.

Torque = Force × Distance from rotation axis

## 3. NUMERICAL APPROACH

These numerical investigations are performed using the open-source solver OpenFOAM (Open-source Field Operation And Manipulation). This solver has been effectively employed in prior researches such as those presented by Tata et al. (2018) where the results have been validated with work published by Eecen and Verhoef (2007). The PIMPLE algorithm for pressure-velocity coupling (Piso Implicit Pressure-Linked Equation) is used. The diffusion term is discretized by the Gauss Linear Upwind grad (U) scheme. The convective term is discretized by the Gauss linear scheme. An explicit Euler scheme is used to calculate the temporal derivative. The time step corresponds to the time that the rotor takes to turn one degree. However, OpenFOAM automatically readjusts the initial value of the time step to maintain the courant number below 1.

$$CFL = \frac{V \times \Delta t}{y_p} < 1$$

## 3.1 Computational Domain and Boundary Conditions

The two-dimensional computational domain is O-H and spans 33D in width and 16D in height. The origin of the coordinates is located at 8D from the left, bottom and top boundaries. The rotor is located in the O subdomain which rotates at the wind turbine rotational speed. The remaining part of the domain is fixed (Fig. 2). An arbitrary mesh interface (AMI) condition is applied to link the O-rotating part of the domain with the domain which remains
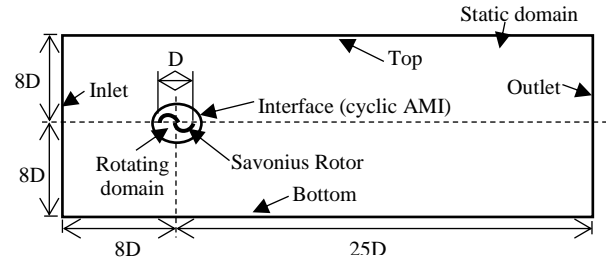


**Fig. 2 Calculation domain and boundary conditions**

fixed. This approach makes it possible to preserve the mesh quality around the rotor while simulating the flow through the wind turbine in rotation. AMI technique has been successively applied by Bekhti et al. (2018) and Guerri et al. (2008) who conducted a research on the dynamic stall of wind turbine airfoils. Guerri et al. (2007) utilized the ASI technique to simulate the fluid flow through a vertical axis wind turbine. This technique is still in use and has recently been applied to the resolution of more complex problems (Duan & Wang 2020; Durrwachter et al., 2021)

The inlet condition with a uniform velocity profile is defined at the left, top, and bottom boundaries of the calculation domain. The outlet condition is applied at the right boundary. A wall condition is applied on the Savonius rotor.

## 3.2 Computational Grid

The computational grid shown in Fig. 3 is built with a hybrid mesh which consists of a blending of structured and unstructured meshes (Tata et al., 2018). An unstructured triangular mesh is utilized for the rotating zone, while a structured quadrilateral mesh is employed for the fixed zone (Bekhti et al. 2019). The boundary layer mesh consists of 13 layers on the concave part of the blade and 20 layers on the convex part of the blade, with a growth factor equal to 1.05. The turbulence model is applied with a wall law, which requires y+ values in the range $30 < y+ < 300$. Numerical simulations are first performed to check the independence of the solution from the mesh. For that purpose, four grid resolutions have been considered: coarse mesh built with 59025 cells, medium mesh with 73461 cells, and fine and very fine meshes, with 114669 and 137434 cells respectively.

These computations are conducted for a traditional Savonius rotor. The Free Stream Wind Speed (FSWS) is set to 7.2 m/s as in Dobrev and Massouh (2011) to compare these numerical results with their experimental data. The wind turbine's rotational speed, determined by the O-subdomain rotational speed, is equal to 500 RPM. With these settings, the Reynolds number, based on the diameter of the rotor, is approximately 105 000 and the tip speed ratio is set at TSR = 0.8. The torque coefficient values computed using the four grids are summarized in Table 3 which shows that the averaged torques calculated with medium, fine, and very fine grids differ slightly. Therefore, the medium grid has been selected for the subsequent calculations.
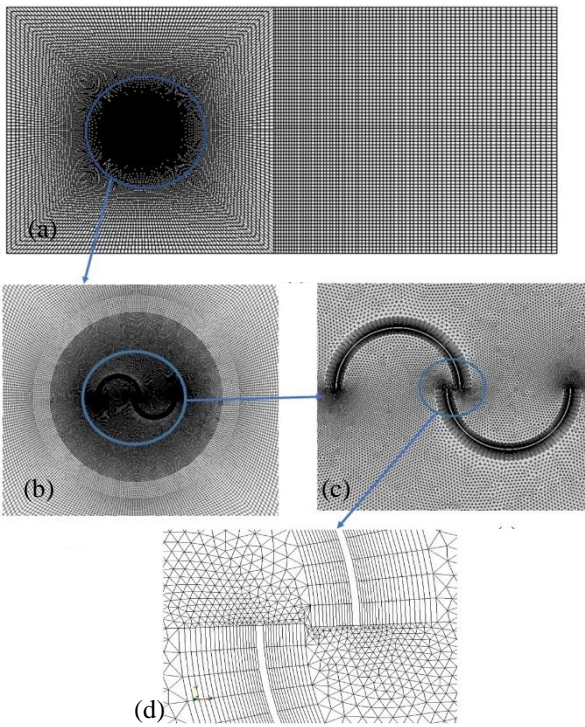
**Fig. 3 Layout of the computational grid (a) the entire domain, (b) around the interface, (c) around the rotor, (d) near the blade wall**

**Table 3 Grid resolution**

| Grid resolution | Number of cells | Average torque coefficient | Error (%) |
|---|---|---|---|
| Coarse | 59 025 | 0.146 | 12.6 |
| Medium | 73 461 | 0.167 | 1.2 |
| Fine | 114 669 | 0.165 | 0.6 |
| Very fine | 137 437 | 0.164 | - |

### 3.3 Validation Study

The traditional Savonius rotor is also considered to validate the applied numerical approach. The free stream wind velocity is set as previously to FSWS=7.2 m/s but computations are performed for various tip speed ratios. These numerical simulations are conducted up to the physical time of 5 seconds, which corresponds to more than 40 rotor revolutions.

The time variation of the torque depicted in Fig. 4 for TSR = 0.8 shows that the solution stabilizes from a physical time equal to 0.25 seconds, which means that the solution converges from two rotations of the rotor. As expected, from this time, the curve of variation of the mechanical torque produced by the rotor versus time is pseudo-sinusoidal.

The power output is determined using the following equation:

$$P = T \cdot \Omega$$

Where only the mean value of one cycle is taken into account. The expected power coefficient is computed for various tip speed ratios (TSR). The free-stream wind
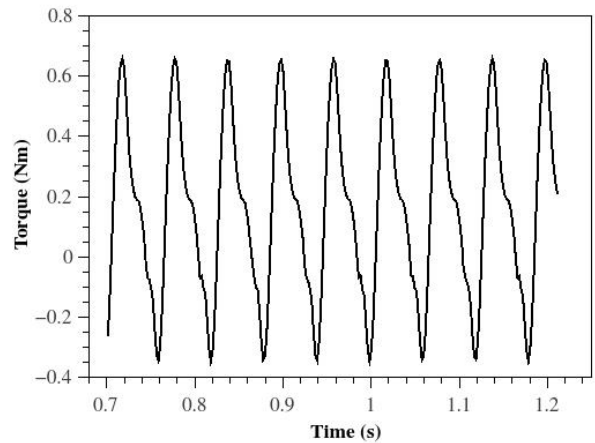


**Fig. 4 Temporal variation of the torque computed for TSR=0.8**

velocity remains constant at 7.2 m/s, while the rotational velocity of the turbine changes. As the AMI technique is applied, the wind turbine's rotational velocity is determined by the velocity of the moving part of the calculation domain. Therefore, the circular part's rotational speed of the calculation domain varies with TSR. The obtained results are compared in Fig. 5 to the experimental data of Dobrev and Massouh (2011). It can be observed that the numerical values closely match the results of the experimental study. The relative average error between the two sets of values is 7%. Figure 5 indicates that the calculated optimum power coefficient is $Cp_{max} = 0.19$, the corresponding tip speed ratio being equal to 1. This result is similar to those obtained by Fujisawa (1992) and Kamoji et al. (2008) who conducted experimental investigations on different Savonius rotors in an open-section wind tunnel. The highest power coefficient measured was $Cp_{max} = 0.17$ and 0.18 for Fujisawa (1992) and Kamoji et al. (2008), respectively at the corresponding tip speed ratio TSR=1. In both references, the rotor aspect ratio was H/D = 1 while the Reynolds number Re = 110000 in Fujisawa (1992) and Re = 120000 in Kamoji et al. (2008).
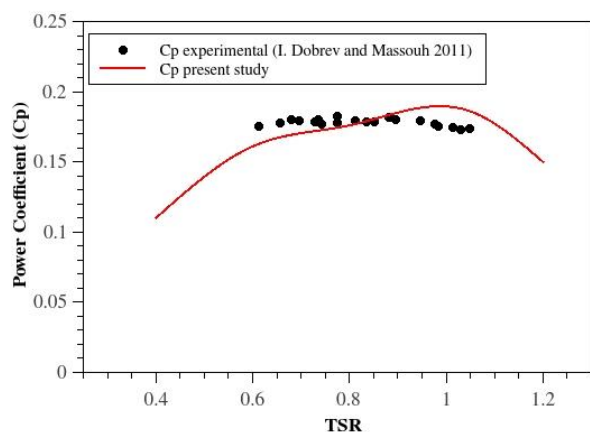


**Fig. 5 Variation of the power coefficient Cp with TSR – Validation study**

**Table 4 Geometrical equations of the blade shapes**

| Profile | | |
|---|---|---|
| Profile 1 | $\forall x$ | $y = 0.0093 - 1.678x - 40.74x^2 - 1079.60x^3 + 2974.13x^4 + 7211.79x^5$ |
| Profile 2 | $-0.1097 \leq x \leq -0.1092$ | $y = 1.44 + 13.13x$ |
| | $-0.1092 \leq x \leq 0.0049$ | $y = 0.0042 - 0.78x - 19.54x^2 - 618.58x^3 - 11094.24x^4 - 96885.45x^5 - 342427.31x^6$ |
| Profile 3 | $-0.107 \leq x \leq -0.104$ | $y = 2.51 + 52.15x + 256.85x^2$ |
| | $-0.104 \leq x \leq 0.006$ | $y = 0.0038 - 0.661x + 8.111x^2 + 535.72x^3 + 7432.55x^4 + 35142.36x^5$ |
| Profile 4 | $\forall x$ | $y = 0.0077 - 1.28x - 25.47x^2 - 251.13x^3 - 1184.47x^4$ |
| Profile 5 | $\forall x$ | $y = 0.0057 - 1.155x + 14.072x^2 + 785.82x^3 + 9726.08x^4 + 42156.11x^5$ |
| Profile 6 | $-0.106 \leq x \leq -0.105$ | $y = 0.69 + 6.47x$ |
| | $-0.105 \leq x \leq 0.0054$ | $y = 0.0045 - 0.77x + 2.96x^2 + 1077.87x^3 + 40467.79x^4 + 680130.3x^5 + 5378924.97x^6 + 16411339.76x^7$ |
| Profile 7 | $-0.111 \leq x \leq -0.109$ | $y = 48.37 + 882.85x + 4027.43x^2$ |
| | $-0.109 \leq x \leq 0$ | $y = 0.00039 - 0.98x - 38.61x^2 - 1741.21x^3 - 33725.24x^4 - 286952.73x^5 - 922665.59x^6$ |

# 4. RESULTS AND DISCUSSION

In the subsequent section, the impacts of the blade profile on the aerodynamic efficiencies of a single Savonius turbine are evaluated. Thereafter, the performances of elliptical blade twin-rotors are estimated. In the following computations, the free stream wind velocity is set to 7.2 m/s.

## 4.1 Effect of the Blade Profile on the Performances

Seven profiles, named profile 1 to profile 7, are considered (Fig. 6). Profile 1 is a V-shaped profile considered by El-Askary et al. (2018). Profile 2 takes its foundation from the Sivasgaram profile (Sevasegaram, 1978). Profile 3 is derived from the Benesh profile shape (Benesh, 1988). Profile 4 is the incurved shape studied by Driss et al. (2014). Profile 5 is an elliptical shape considered by Kacprzak et al. (2013) and Profile 6 is a new elliptical shape proposed by Alom et al. (2016). The seventh profile is a Bach shape (Bach, 1931).

The equations describing the profiles' geometries can be found in Table 4, the rotor is positioned at the origin of the coordinate system.

### 4.1.1 Power and Torque Coefficients

The aerodynamic performances of the different blade shape rotors are contrasted with those of the classic semi-circular wind turbine. The characteristic curves of $C_P$ versus the tip speed ratios are depicted in Fig. 7 for the various Savonius rotors. As reported in previously published studies, it is evident that the traditional Savonius rotor with semicircular blades exhibits the lowest power coefficient. Figure 7 illustrates that the Savonius rotors constructed with profiles 2, 4, 6, and 7 exhibit higher power coefficient values. Wind turbine with profile 7 is efficient at low TSRs, whereas profiles 2, 4, and 6 are most efficient at higher TSR values. The maximal power coefficients ($C_{P, Max}$) values are summarized in Table 5 which shows that the most efficient profile is the number 6 with an average $C_P$ equal to 0.21. Contrasted to that of the classic semicircular profile, $C_{p, Max}$ is improved by 80% for profile 6 based on the new elliptical profile, to 75% for profile 2 and 65% for profile 4.

Figure 8 displays the characteristic curve of the torque coefficient plotted against the tip speed ratio (TSR) for the different Savonius rotors. For all blade profiles, it is obvious that the torque coefficient decreases as TSR increases. As noticed for the power coefficient, at low TSRs, the highest torque coefficient is provided by profile number 7. For TSRs ranging from 0.8 to 1.2, the torque is higher for the rotors built with profiles 2, 4, and 6. Figure 9 depicts the fluctuation of the torque versus the angular position during one complete revolution of the rotor. This diagram displays four notable torque extremes, including two peaks occurring at angular positions ranging from 30° to 60° and 210° to 240°, as well as two minimum values at angular positions within the range of 150°-170° and 330°-350°.It is observed that the peak torque value is attained when the blade aligns with the flow and that the torque coefficient drops to a minimum value at the blade positions normal to the incident wind. Besides, the maximum torque is provided by profile 7.

**Table 5 Comparison of the $C_{P, max}$ of the different rotors**

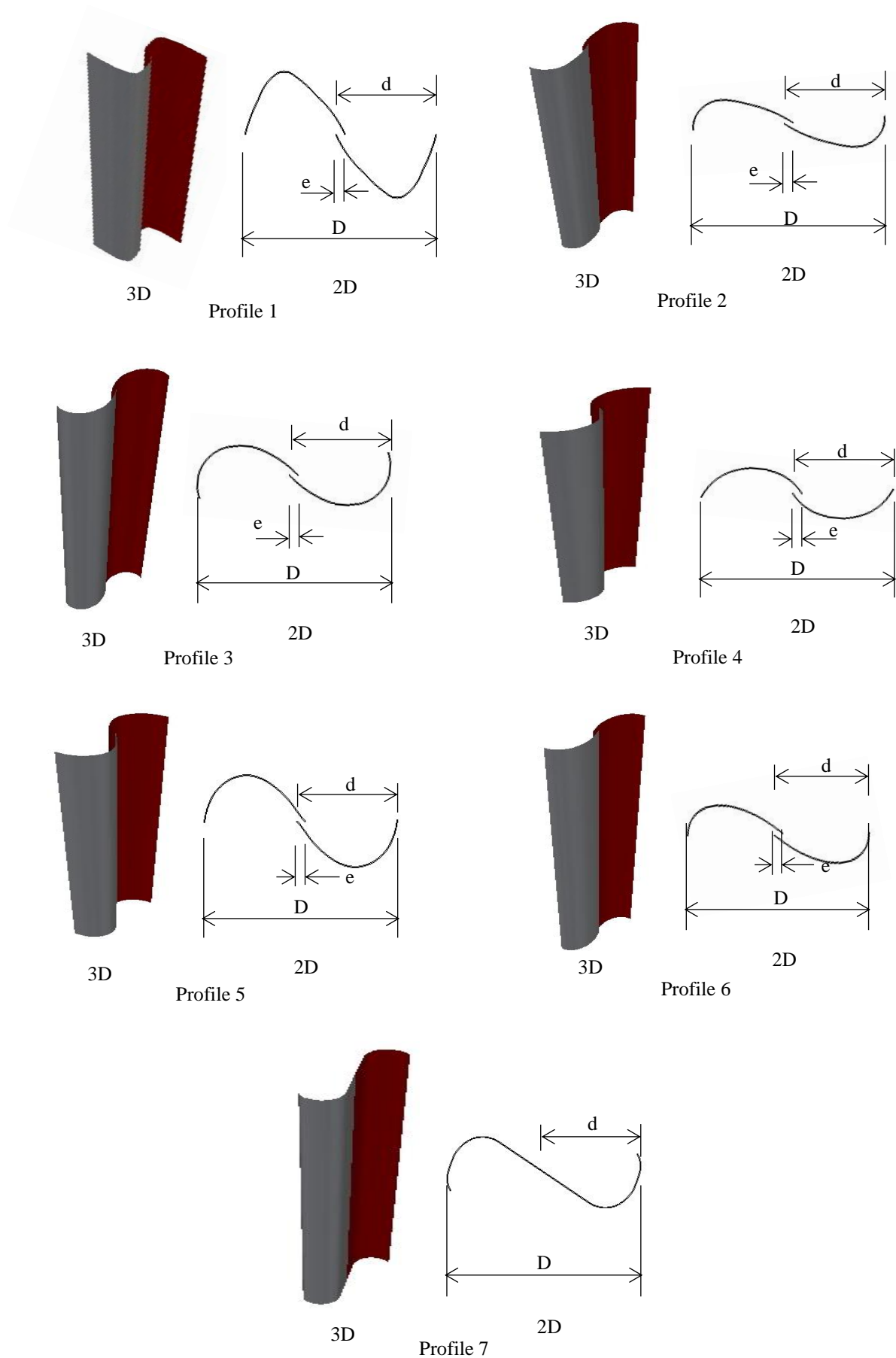| Profile | $C_{P, max}$ | TSR ($C_{P,max}$) | Gain (%) | Remarks |
|---|---|---|---|---|
| SC | 0.186 | 1 | - | Conventional blade, Cp lower than 0.2 |
| 1 | 0.205 | 1 | 10 | Cp higher than 0.2 |
| 2 | 0.336 | 1 | 75 | Cp higher than 0.3 |
| 3 | 0.216 | 0.6 | 29 | Cp higher than 0.2 at low TSR |
| 4 | 0.312 | 1 | 65 | Cp higher than 0.3 |
| 5 | 0.227 | 0.6 | 24 | Cp higher than 0.2 at low TSR |
| 6 | 0.342 | 1.2 | 80 | Highest Cp at high TSR |
| 7 | 0.328 | 0.6 | 49 | High Cp and highest $C_T$ at low TSR. High static torque. |

**Fig. 6 Blades profiles considered in the current investigation (Profile 1 (El-Askary et al., 2018), Profile 2 (Rahai, 2005), Profile 3 (Benesh, 1988), Profile 4 (Driss et al., 2014), Profile 5 (Kacprzak et al.,2013), Profile 6 (Alom et al. 2016) and Profile 7 (Bach, 1931)**
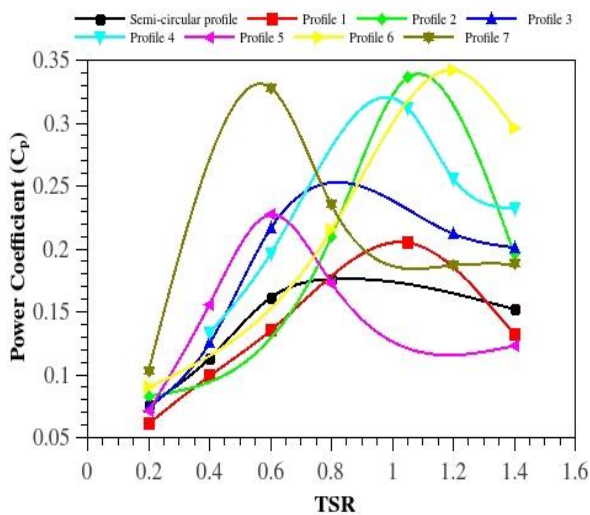
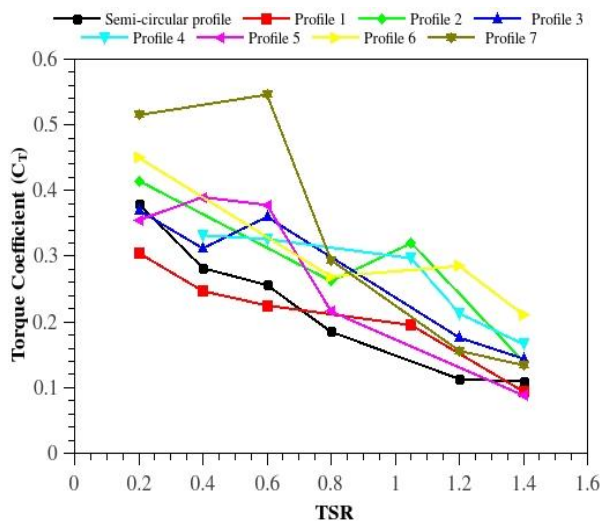**Fig. 7 Power Coefficient C_P versus TSR for the different Savonius rotors**



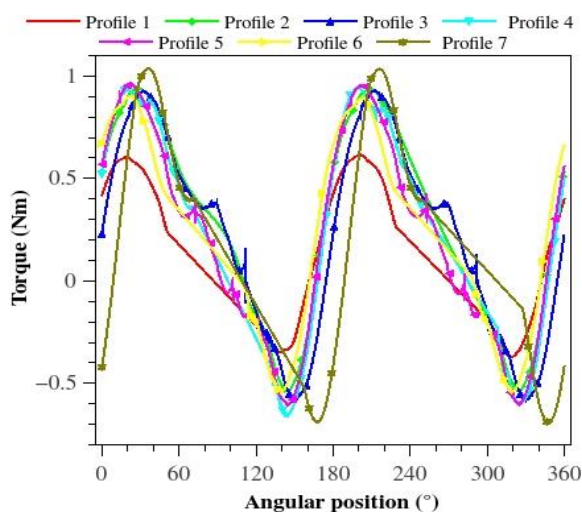**Fig. 8 Torque Coefficient C_T versus TSR for the different Savonius rotors**



**Fig. 9 Variation of the torque coefficient versus the angular position - TSR = 1.05**

### 4.1.2 Velocity fields

The outcomes of these numerical simulations are used to explore the flow structure around the different rotors. Figures 10 and 11 display the velocity magnitude contours in the near wake of various Savonius rotors for the rotor normal to and aligned with the incident flow respectively. These two figures show that the flow around the rotors is that of a bluff body with a wake flow downstream of the rotors characterized by wake velocities lower than the free flow velocity. Moreover, a detachment of vortices from the blade tips is seen. These detached vortices are characterized by an accelerated airflow that propagates in the wake region. In addition, flow accelerations in the spacing between the blades are observed. The airflow passing through this gap is directed towards the blade's concave side that is returning, leading to a pressure force that mitigates the unfavorable torque produced by this blade's motion and contributes to the wind turbine rotation. It's also evident that in the scenario of the rotors with profile 7, the flow is concentrated at the ends of the blades, hence putting more pressure on the blades, which explains the higher torque.

For all blade profiles, at the 90° angular position, there is a noticeable difference between the velocities of the convex and concave parts of the advancing blade, with higher velocities on the convex sides. This difference in velocity results in a positive torque exerting on the advancing blade. The most significant velocity contrast between the concave and convex parts of the advancing blade is identified in profiles 2, 4, and 6. Conversely, still for all the profiles, near the returning blades, the velocities are higher on the convex part compared to the concave part. These velocity differences generate an undesirable negative torque. However, the overall torque remains positive, contributing to the rotational motion of the rotor. Figure 10 shows that profile 4 has the smallest velocity difference around the returning blade.

The point of stagnation on the returning blade counteracts the positive torque resulting from the advancing blade. Compared with the other profiles, in the scenario of profile 7, the point of stagnation is shifted closer to the rotor center, and the zone characterizing the flow near the stagnation point is reduced. This displacement of the stagnation region to the center of rotation reduces the negative torque generated by the returning blade and therefore enhances the effectiveness of the wind turbine. The highest velocities and lowest pressures are located where the blade is parallel to the flow. Figure 10 shows also that the flow separation starts at the points where the velocity on the blade is highest and that the wake region exhibits a significant size. This is due to the increased blocking of the flow area. The velocity fields are similar for all profiles except for profile 4 for which the velocity deficit within the near wake is of lesser significance. However, the complex flow pattern downstream of the rotor holds significant importance in wind farm design and requires increased focus in forthcoming researches.

At the angular position of 180°, where the maximum torque is reached, a noticeable acceleration of the fluid is observed on the convex part of the advancing blade. This
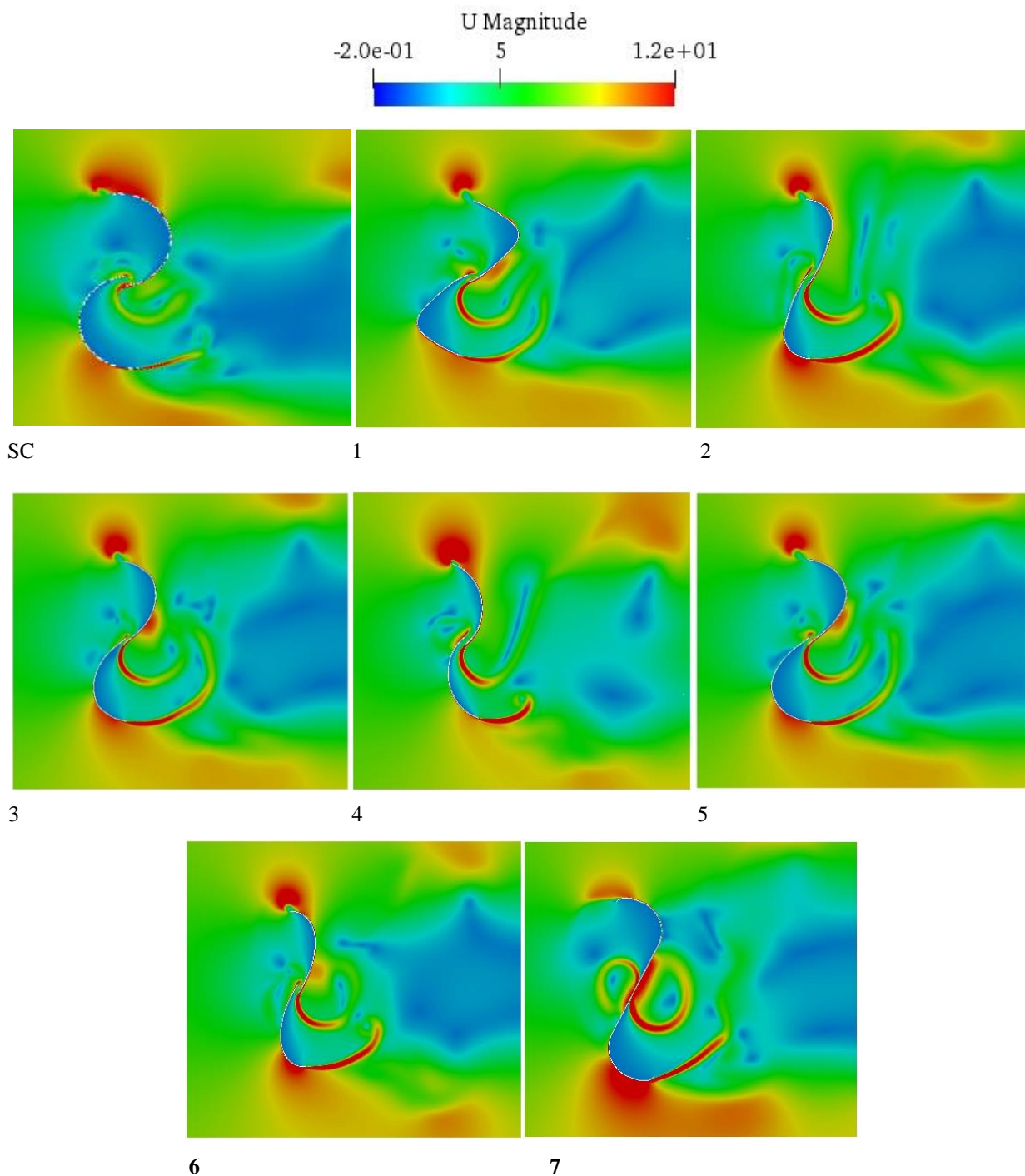
**Fig. 10 Velocity contours surrounding the different Savonius rotors. TSR=1.05 - ϕ=90°**

acceleration actively contributes to the generation of lift force, which propels the turbine rotation. This fundamental phenomenon coexists alongside other recirculation zones present on the concave part of the advancing blade, as well as on both sides of the returning blade.

Figure 12 shows streamlines around the different Savonius rotors at the positions normal to and aligned with the free stream velocity. As in Figs. 10 and 11, a complex flow structure with multiple recirculation areas is noticed. The prevailing and prominent structure is the tip vortex formed at the uppermost tip of the advancing blade, occurring when the rotor aligns at 90° to the incoming

flow. This vortex separates from the blade tip when the rotor is at 180°. Boundary layer separation is also noticeable on the advancing blade, particularly near the turbine's axis of rotation, occurring when the rotor reaches a position of 180°. The vortices are released from the surface of the blade when the rotor is at 90°.

**4.1.3 Pressure Contours**

Figures 13 and 14 illustrate the pressure fields around the different Savonius rotors at the positions of 90° and 180° respectively. When the rotors are at 180°, for almost blade profiles, a stagnation point is evident at the tip of the advancing blade. A negative pressure gradient becomes
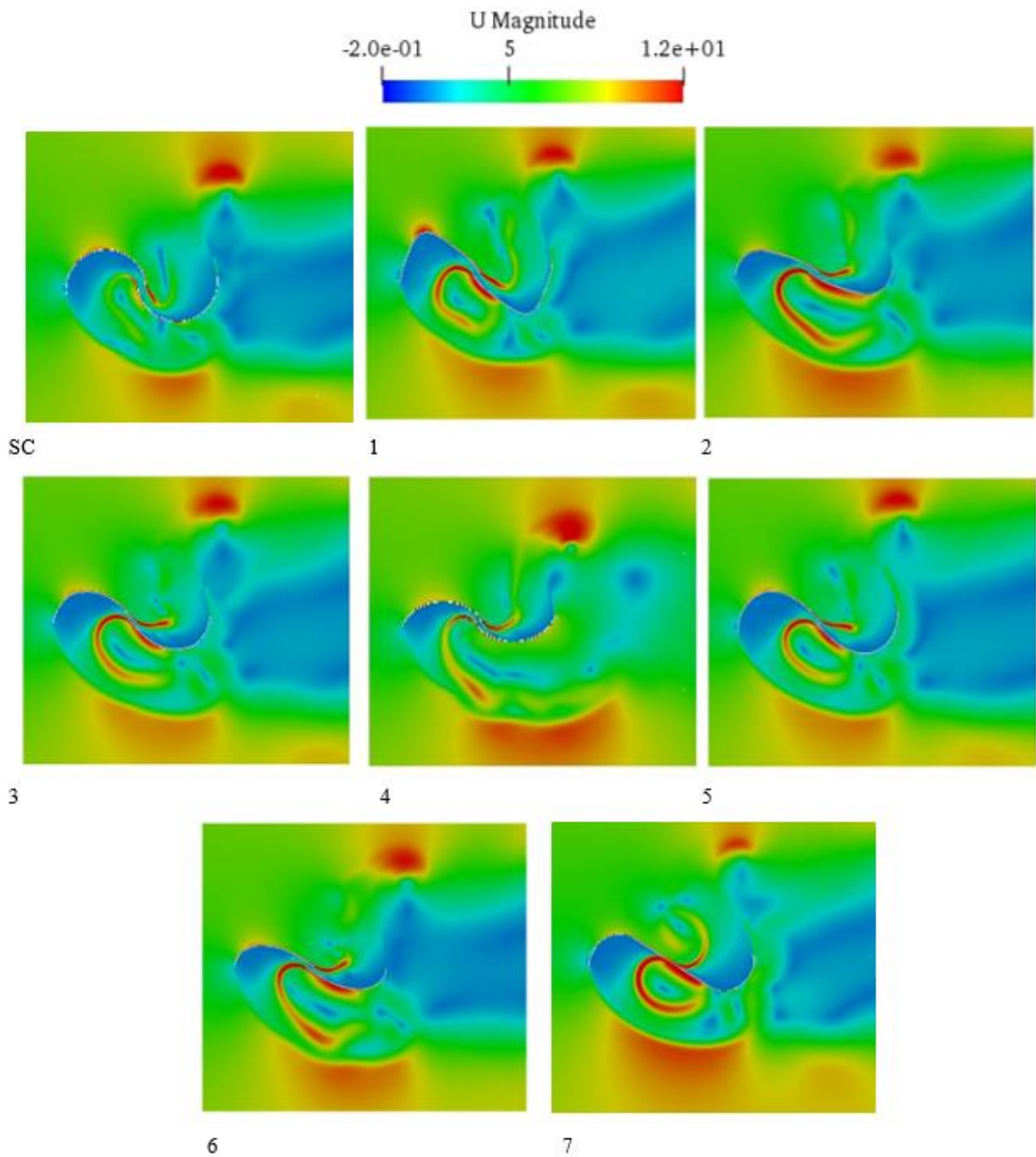
**Fig. 11 Velocity contours surrounding the different Savonius wind rotors. TSR=1.05 - ϕ=180°**

apparent in the downstream region of the rotor, resulting in flow separation and recirculation, which leads to the formation of a highly turbulent area in the wake of the turbine. A wake zone is thereby created downstream of the Savonius rotor. As the flow separates, the pressure within the wake area is still at a low level. Higher pressure values are found upstream of the rotor while the low pressure region is developed downstream. This pressure gradient creates a pressure drop which causes the turbine to rotate. At the 90° position, the returning blade of profile 7 experiences a high-pressure zone near the shaft on its convex side, alleviating the adverse torque effect and encourages the generation of a more favorable positive torque for the rotor. Conversely, a substantial low-

pressure area is evident in the proximity of the convex part of the advancing blades, specifically for profiles 2, 4, and 6. This low-pressure zone enhances the torque generated by the rotor. Furthermore, the pressure on the concave part of the advancing blade is greater than the pressure on the convex part, creating a pressure difference that results in a forward thrust on the advancing blade. The most significant pressure disparity around the advancing blade is observed for profiles 2, 6, and 7. However, on the returning blade, the pressure is greater on the convex part when compared to the concave side, resulting in a negative torque which reduces the overall torque. Profile 7 has the lowest pressure difference around the returning blade.
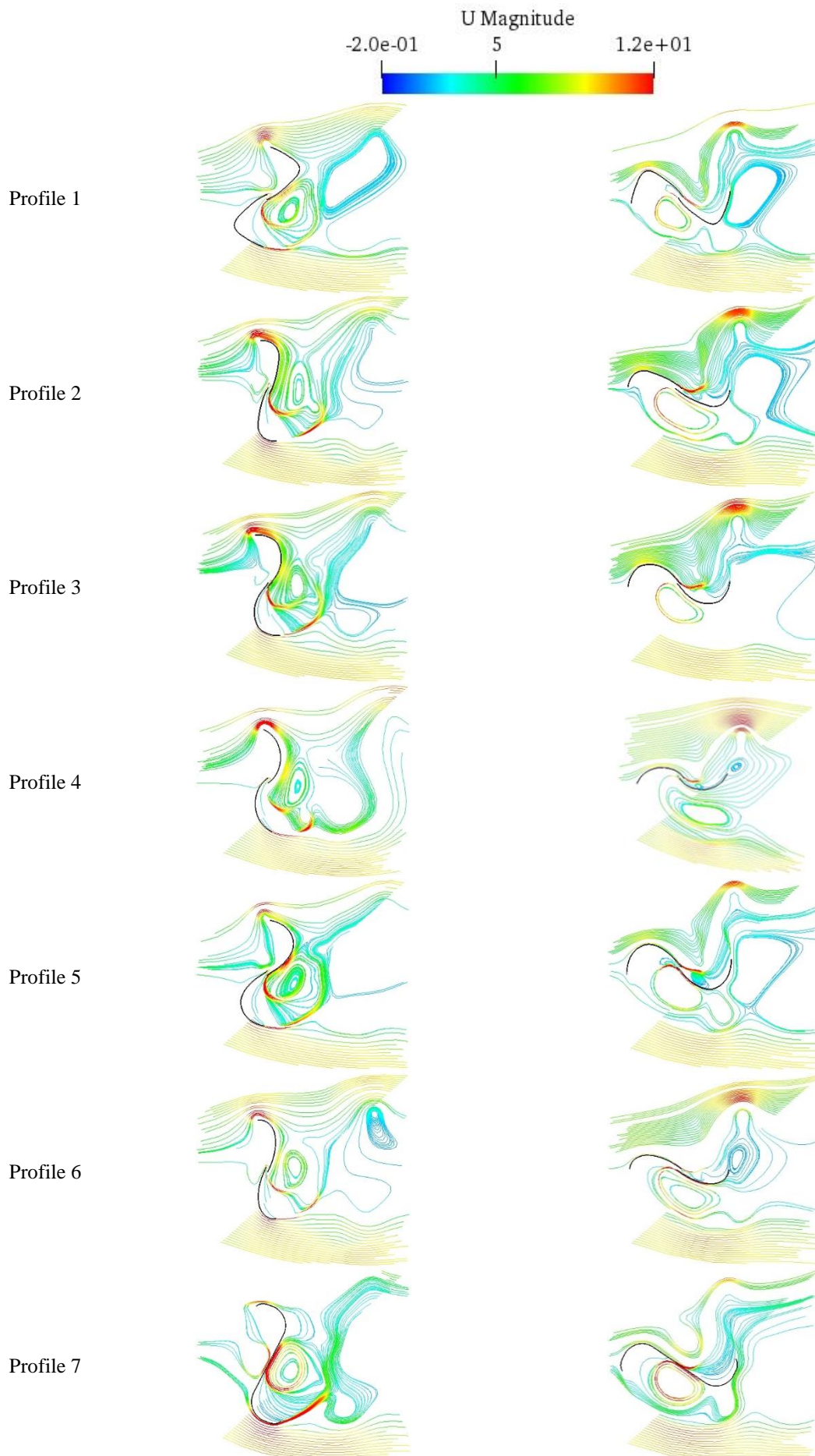
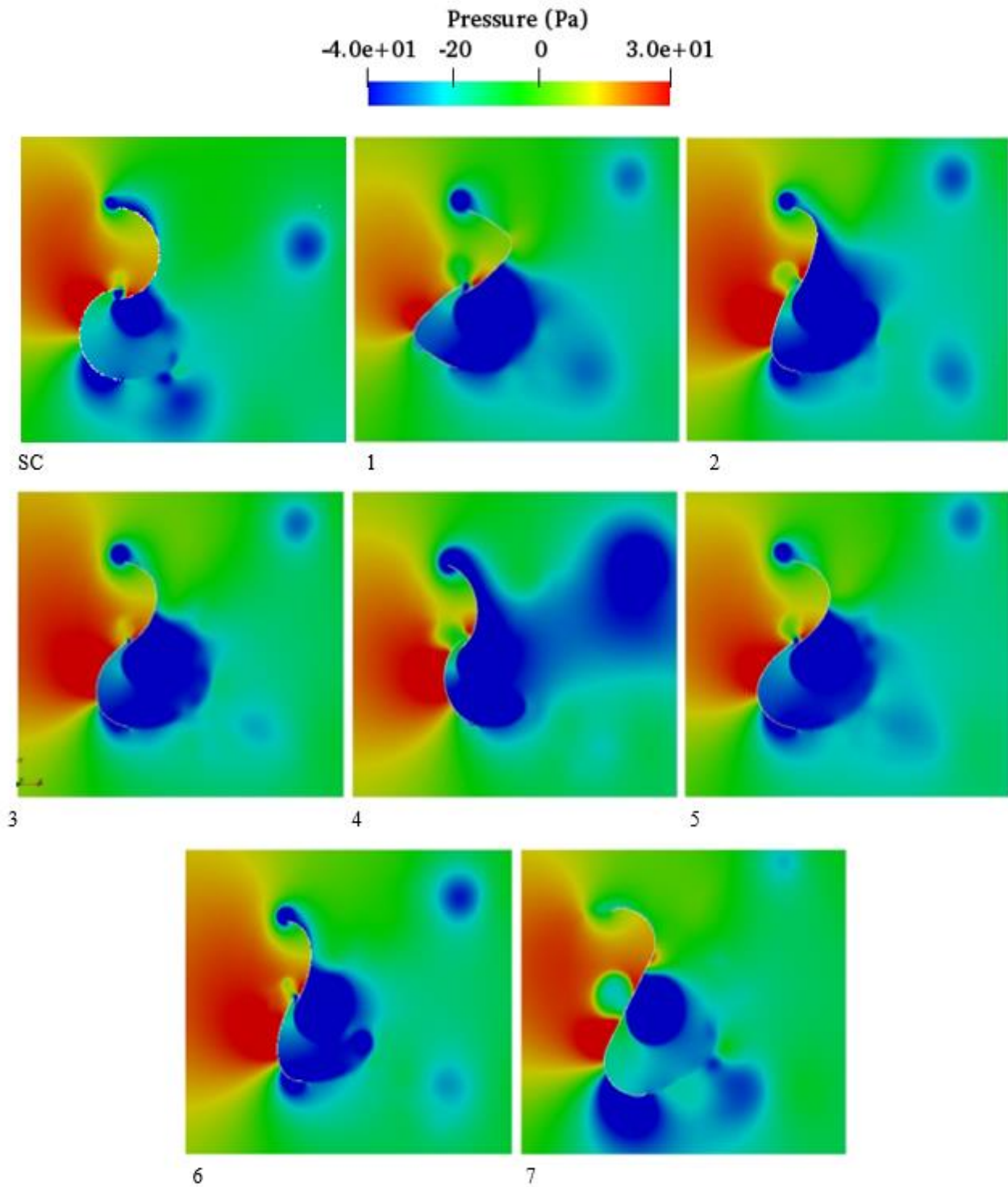**Fig. 12 Streamlines around the different Savonius rotors at ϕ=90° (left) and 180° (right). TSR=1.05**

**Fig. 13 Pressure fields around the different Savonius rotors - TSR=1.05 - ϕ=90°**

In summary, the pressure and velocity fields illustrate that the maximum velocities and minimum pressures occur at points where the blades are parallel to the flow and that the Savonius rotor performs best with the profiles that tend to direct the flow toward the blades tips, putting more pressure on the blades and, therefore, generating higher torque. The semicircular profile has a significantly larger area of the blade compared to profiles 2, 4, and 6. Consequently, the returning blades of profiles 2, 4, and 6 have much less negative drag than the semicircular profile.

## 4.2 Twin-Rotor with Elliptical Blades

It was demonstrated in the literature review that the interaction between two Savonius rotors with semicircular blades placed side by side improved the efficiency of wind turbines. Some authors have shown that if the gap between the two rotors is optimized, the wind turbines' power coefficient can increase by 110% to reach the value of 0.21. In the following, to further enhance the effectiveness of the twin rotors, two Savonius wind turbines with elliptical blades are considered. The studied configuration
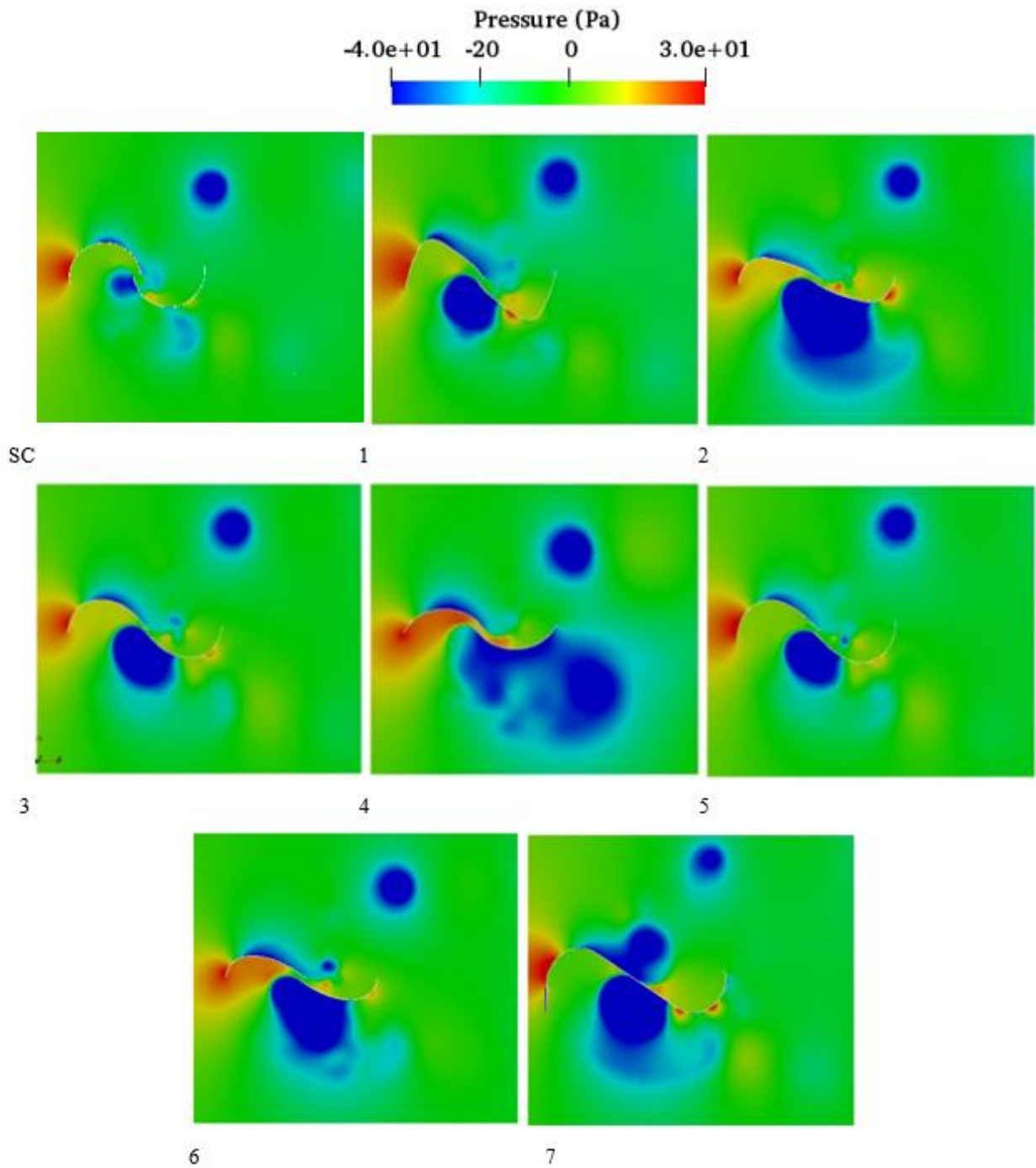
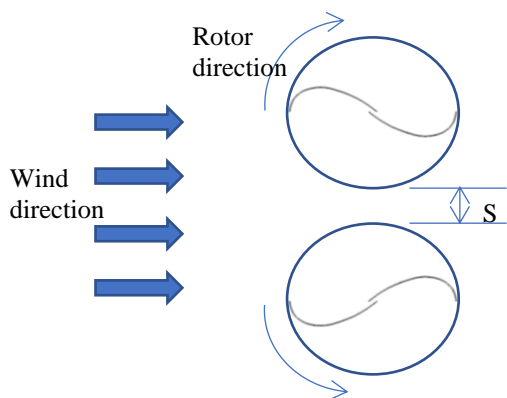**Fig. 14 Pressure fields around the different Savonius rotors TSR=1.05 - ϕ = 180°**



**Fig. 15 Twin rotor configuration**

is two counter-rotating rotors built with profile 6, spaced by $S_t = 0.2D$, and rotating in phase (Fig. 15).

### 4.2.1 Power and Torque Coefficients of the Dual-Rotor Configuration

Figure 16 illustrates the power coefficient variation (CP) for the dual-rotor in relation to the Tip-Speed Ratio (TSR). A noticeable enhancement of 9% is observed in the dual-rotor's power coefficient configuration, compared to the similar single rotor with profile number 6. It can also be noticed in Fig. 16 that for TSR greater than 1.2, the effectiveness of the twin rotor falls below the single rotor efficiency.
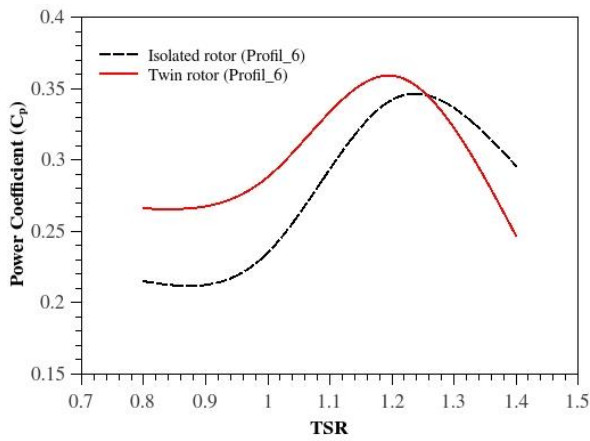
**Fig. 16 Twin-rotor's power coefficient versus TSR**



**Fig. 18 Variation of the torque of the twin-rotor versus angular position**
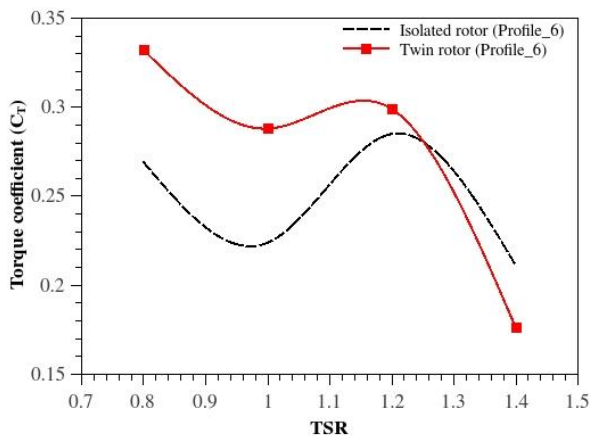


**Fig. 17 Twin-rotor's torque coefficient versus TSR**

The torque coefficient variation versus TSR represented in Fig. 17 illustrates that the maximum dual-rotor's torque coefficient experiences a noteworthy enhancement of 10% contrasted to the single rotor with profile number 6. However, as for the power coefficient, at TSR values greater than 1.2, the torque generated by the dual rotor is comparatively lower than that produced by a single rotor using the same profile 6.

Figure 18 depicts the torque variation in relation to the angular position across a full revolution of the rotor for the twin-rotor and single-rotor configurations. It's evident that the dynamic torque generated by the twin rotor surpasses that of the isolated rotor. Analysis of the results shows the torque is enhanced by 37% compared to the single rotor with profile 6.

The velocity magnitude fields, streamlines, and pressure contours are represented in Fig. 19 with the twin-rotor at two angular positions, 90° and 180°.

**4.2.2 Flow Field**

As for the isolated rotor, in Fig. 19 (a), it is evident that the flow structure is intricate and varies with the rotor's position. The velocity fields show that the flow structure is symmetrical, with the generated wake being larger and wider contrasted to that of an isolated rotor. This observation suggests that the turbines have greater drag, which is advantageous for enhancing the Savonius
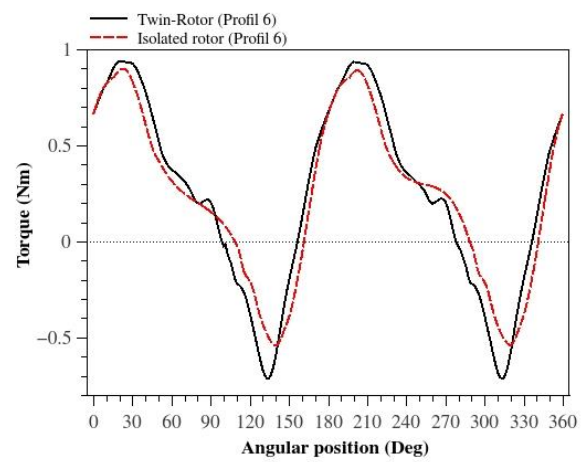
turbines' efficiency. At the angular position of 180°, where the maximum torque is achieved, fluid accelerations are noticeable on the convex part of the advancing blades for both rotors. These accelerations contribute to the generation of the lift force. Recirculation zones form on the concave sides of the advancing blades and on both parts of the returning blades. At the angular position of 90°, the stagnation point on the returning blades of both rotors counterbalances the positive torque generated by the concave parts of the advancing blades. At the advancing blades' tips, a higher velocity is observed, resulting in more pronounced vortex shedding. Additionally, the wind velocity at the upwind side of the twin rotor is greater than that of an isolated rotor, mainly due to the interaction between the turbines. In both angular positions, flow acceleration between the two rotors is seen. This leads to a decrease in the high-pressure area on the convex parts of the returning blades, resulting in a reduction of the negative torque and ultimately contributing to an increase in the overall torque of the turbine. Therefore, the reciprocal interaction between the rotors within the dual-rotor setup imparts a positive effect on the effectiveness of the Savonius wind turbine.

The streamlines depicted in Fig. 19 (b) reveal a notable degree of complexity in the flow structure, marked by the presence of multiple recirculation zones. The prevailing and prominent structure is the tip vortex formed at the uppermost tips of the advancing blades at the angular position of 90° and grows downstream and separates from the blade tips at the angular position of 180°. A separation of the boundary layer is seen to form on the advancing blade, near the turbine rotation axis. This flow detachment starts forming at the angular position of 0° and is released at the angular position of 90°. Additionally, it is evident that the rotors rotations generate an aerodynamic shield against the flow within the region situated between the rotors. Consequently, the flow is directed from the convex side of the returning blades towards the concave side of the advancing blades. This redirection of the flow contributes to an enhancement in the wind turbine's performance.

Figure 19 (c) shows the pressure fields around the twin rotor with stagnation points at the advancing blades

tips. Greater pressures are noticed on the concave surfaces of the advancing blades when compared to the single rotor configuration. This phenomenon contributes to the superior performance exhibited by the Savonius twin rotor setup.

Table 6 demonstrates that the twin-arrangement rotor's power coefficient, which has been examined in this present study, surpasses the power coefficients obtained in comparable studies documented in the existing literature. Savonius rotors in twin arrangement and elliptical-shaped blades are therefore the most efficient. To the authors' knowledge, this case has not been considered in previously published studies.
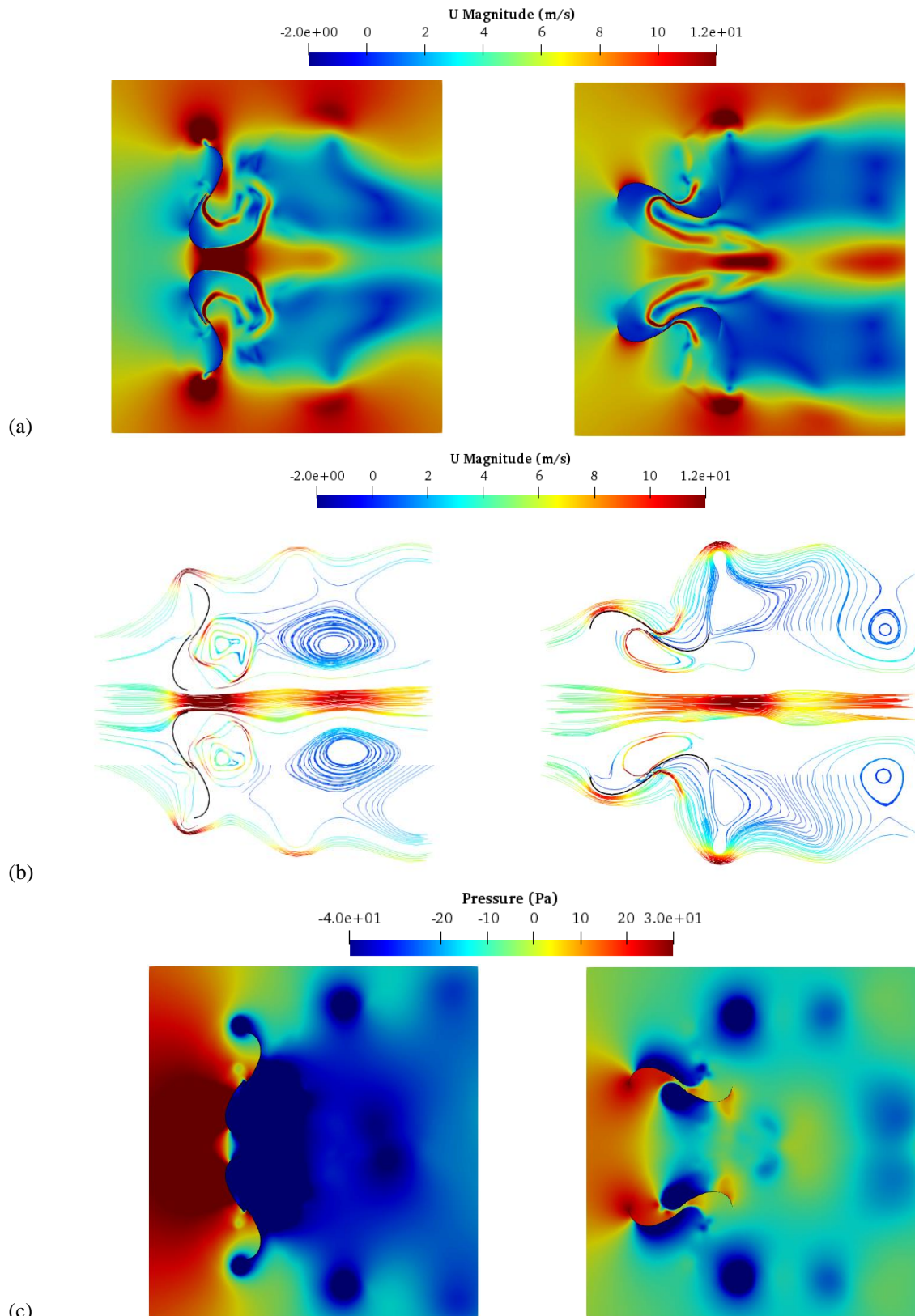


**Fig. 19 Velocity, streamlines, and pressure fields around the twin rotor at 90° (left) and 180° (right)**

**Table 6 Comparison of the current results with those of previous works.**

| Blade Profile | Configuration | Researchers | Cp$_{max}$ |
|---|---|---|---|
| Elliptical | Single rotor | Alom et al. (2016) | 0.33 |
| Modified Bach | Single rotor | Alom and Saha (2019a) | 0.315 |
| **Elliptical** | **Single rotor** | **Present study** | **0.34** |
| Semi-circular | Twin-aligned counter-rotating rotors with triangular deflectors in the middle. | Etemadeasl et al. (2021) | 0.266 |
| Semi-circular | Three turbines in a triangular arrangement | Meziane et al. (2019) | 0.28 |
| **Elliptical** | **Twin-aligned counter-rotating rotors** | **Present study** | **0.36** |

## 5. CONCLUSION

In the current study, Aerodynamic performance assessments of vertical axis wind turbines utilizing the Savonius design have been conducted through numerical investigations. The computational analysis involved solving the governing equations represented by the Unsteady Reynolds Averaged Navier-Stokes equations, along with the k-ω SST turbulence model. This was performed within a two-dimensional computational domain. To simulate the flow around the rotating wind turbine, a sliding mesh technique was employed. The validity of the employed approach was established by comparing the power coefficient of a semicircular blade rotor with experimental data provided by Dobrev and Massouh (2011). Additionally, the highest power coefficient was compared to those obtained by Fujisawa (1992) and Kamoji et al. (2008) who conducted experimental investigations on different Savonius rotors in an open-section wind tunnel.

Then, the impact of the blade shape on the aerodynamic effectiveness of the Savonius turbine was assessed by examining seven distinct blade profiles. The obtained results indicated that the Savonius wind turbine equipped with the elliptical blade (profile 6) yielded the highest power coefficient whose maximum Cp is 0.34 at the tip speed ratio TSR = 1.2. The increase in Cp, when contrasted to the wind turbine equipped with traditional semi-circular blades, is approximately 80%. But for low values of TSR ranging from 0.2 to 0.8, a maximum Cp of 0.33 is reached by the wind turbine with a Batch profile (profile 7). These results illustrate that the Savonius rotor has the highest power coefficient with blade profiles that tend to direct the flow towards the blade tips, putting more pressure on the blades and thereby generating more

torque. Moving the stagnation point towards the center of rotation reduces the adverse torque generated by the returning blade and thus enhances the wind turbine performance. Moreover, considering the blade surface, it is noticed that the conventional semi-circular profile covers a larger area of the blade compared to the six other profiles considered in this study. Consequently, the returning blades of these profiles encounter considerably less negative drag than the semicircular profile.

Thereafter, the Savonius wind turbine efficiency, built with the new elliptical blade profile 6, in a twin rotor were evaluated. These results demonstrate enhancements in the coefficients of the power and the torque of the dual-rotor by 9% and 10%, respectively, compared to the effectiveness of the single rotor. However, for TSR values above 1.2, the Cp values of the dual configuration are less than those of the isolated rotors. Conversely, the velocity fields reveal a symmetrical flow structure, with the generated wake being larger and wider contrasted to that of an isolated rotor. This observation suggests that the turbines have greater drag, which is advantageous for enhancing the turbines' efficiency.

### *Future Works*

As a continuation of this work, experimental investigations are planned to validate the obtained results. Simultaneously, additional numerical investigations are planned to evaluate the effectiveness of the Savonius twin wind turbines built with the Batch and other profiles and to examine the impact of the rotor dimensions. Furthermore, the flow's complex structure in the wake of Savonius rotors needs attention in the construction of wind farms. Therefore, the examination of the wake of these wind turbines installed in farms should be considered.

## CONFLICT OF INTEREST

The authors confirm that there are no known conflicts of interest associated with this publication and there has been no significant financial support for this work that could have influenced its outcome.

## AUTHORS CONTRIBUTION

All authors contributed to the present study: **M. Tata**: Conceptualization, Methodology, Validation, Formal analysis, Writing review and editing, Comments; **A. Bekhti**: Methodology, Formal analysis, Writing review and editing, Comments; **M. Maizi**: Validation, Investigation, Writing review and editing, Comments; **N. O. Cherifi**: Software; **A. Tamoum**: Software; **D. Hamane:** Methodology, Validation, Formal analysis, Comments; **A. Boudis**: Investigation, Manuscript writing, Comments; **M. Debbache**: Investigation, Manuscript writing, Comments; **O. Guerri**: Conceptualization, Formal analysis, Comments. All authors read and agreed to the published version of the manuscript.

## REFERENCES

Akwa, J. U., Vielmo, H. A., & Petry, A. P. (2012). A review on the performance of Savonius wind

turbines. *Renewable Sustainable Energy Review, 16*(5), 3054–3064. https://doi.org/10.1016/j.rser.2012.02.056

Al-kayiem, H. H., Bhayo, B. A., & Assadi, M. (2016). Comparative critique on the design parameters and their effect on the performance of S-rotors. *Renewable Energy, 99*, 1306–1317. https://doi.org/10.1016/j.renene.2016.07.015

Alom, N., & Saha, U. K. (2019a). Evolution and progress in the development of savonius wind turbine rotor blade profiles and shapes. *Journal of Solar Energy Engineering*, *141*(3), 030801. https://doi.org/10.1115/1.4041848

Alom, N., & Saha, U. K. (2019b). Influence of blade profiles on Savonius rotor performance: Numerical simulation and experimental validation. *Energy Conversion and Management, 186*, 267–277. https://doi.org/10.1016/j.enconman.2019.02.058

Alom, N., Kolaparthi, S. C., Gadde, S. C., & Saha, U. K. (2016). *Aerodynamic design optimization of elliptical-bladed Savonius-stype wind turbine by numerical simulations.* International Conference on Offshore Mechanics and Arctic Engineering. American Society of Mechanical Engineers. https://asmedigitalcollection.asme.org/OMAE/proceedings-abstract/OMAE2016/49972/281310

Altan B. D., & Gungor, A. (2022). Examination of the effect of triangular plate on the performance of reverse rotating dual Savonius wind turbines. *Processes*, 10.22378. https:// doi.org / 10.3390/pr10112278.

Ashwindran, S. N., Azizudin, A. A., & Oumer, A. N. (2020). A moment coefficient computational study of parametric drag driven wind turbine at moderate tip speed ratios. *Australian Journal of Mechanical Engineering*. *20*(2), 433-447. https://doi.org/10.1080/14484846.2020.1714364

Bach, G. (1931). Untersuchungen uber savonius rotoren und verwandte stromungsmaschinen. *Forschung Auf Dem Gebiet Des Ingenieurwesens A, 2*(6), 218–231.

Banerjee, A., Roy, S., Mukherjee, P., & Saha, U. K. (2014). *Unsteady flow analysis around an elliptic bladed Savonius style wind turbine* Gas Turbine India Conference. American Society of Mechanical Engineers.

Bekhti, A., Maizi, M., Guerri, O., Laazab, S., Bouzidi, S. C., & Boumerdassi, K. (2018, November). *Numerical analysis of dynamic stall on wind turbine airfoils* International Conference on Wind Energy and Applications in Algeria. IEEE.

Bekhti, A., Maizi, M., Tata, M., & Laazab, S. (2019, November). *Numerical Investigation of Turbulent Flow over a Vertical axis Wind Turbine* 7th International Renewable and Sustainable Energy Conference. IEEE.

Benesh, A. H. (1988). *Wind turbine system using a vertical axis Savonius type rotor.* U.S. Patent No: US5494407A.

Bhayo, B. A., & Al-kayiem, H. H. (2017). Experimental characterization and comparison of performance parameters of S-rotors for standalone wind power system. *Energy, 138*, 752–763. https://doi.org/10.1016/j.energy.2017.07.128

Chan, C. M., Bai, H. L., He, D. Q. (2018). Blade shape optimization of the Savonius wind turbine using a generic algorithm. *Applied Energy, 213*, 148–157. https://doi.org/10.1016/j.apenergy.2018.01.029

Chen, L., Chen, J., & Zhang, Z. (2018). Review of the savonius rotor's blade profile and its performance. *Journal of Renewable and Sustainable Energy*, *10*, 013306. https://doi.org/10.1063/1.5012024

Dewan, A., Gautam, A., & Goyal, R. (2021). Savonius wind turbines: A review of recent advances in design and performance enhancements. *Materials Today: Proceedings*, *47*, 2976-2983. https://doi. org / 10.1016 / j.marpr.2021.05.205

Diaz, A. P., Parajo, G. J., & Salas, K. U. (2015). Computational model of Savonius turbine. *INgeniare. Revista chilena de Ingenieria*, *23*(3), 406–412. https://doi.org/10.4067/S0718-33052015000300009

Dobrev, I., & Massouh, F. (2011). CFD and PIV investigation of unsteady flow through Savonius wind turbine. *Energy Procedia*, *6*, 711–720. https://doi.org/10.1016/j.egypro.2011.05.081

Driss, Z., Mlayeh, O., Driss, D., Maaloul, M., & Abid, M. S. (2014). Numerical simulation and experimental validation of the turbulent flow around a small incurved savonius wind rotor. *Energy*, *74*, 506–517. https://doi.org/10.1016/j.energy.2014.07.016

Duan, Z., Jia, F., & Wang, Z. J. (2020). *Sliding mesh and arbitrary periodic interface approaches for the high order FR/CPR method*. AIAA Scitech 2020 Forum. Orlando, FL. https://doi.org/10.2514/6.2020-0086

Dürrwächter, J., Kurz, M., Kopper, P., Kempf, D., Munz, C. D., & Beck, A. (2021). An efficient sliding mesh interface method for high-order discontinuous Galerkin schemes. *Computers & Fluids*, *217*, 104825, https://doi.org/10.1016/j.compfluid.2020.104825.

Ebrahimpour, M., Shafaghat, R., Alamian, R., & Shadloo, M. S. (2019). Numerical inverstigation of the Savonius vertical axis wind turbine and evaluation of the effect of the overlap parameter in both horizontal and vertical directions on its performance. *Symmetry*, *11*(6), 821. https://doi.org/10.3390/sym11060821

Eecen, P. J., & Verhoef, J. P. (2007). *EWTW Meteorological Database Description*. ECN-E—07-041, ECN Windenergy, Netherlands

El-Askary, W. A., Saad, A. S., AbdelSalam, A. M., & Sakr, I. M. (2018). Investigating the performance of a twisted modified Savonius rotor. *Journal of Wind*

*Engineering & Industrial Aerodynamics*, *182*, 344–355. https://doi.org/10.1016/j.jweia.2018.10.009

El-Baz, A. R., Youssef, K., & Mohamed, M. H., (2016). Innovative improvement of a drag wind turbine performance. *Renewable Energy*, *86*, 89–98. https://doi.org/10.1016/j.renene.2015.07.102

Etemadeasl, V., Esmaelnajad, R., Farzaneh, B. & Jafari, M. (2021). Application of counter rotating rotors for improving performance of savonius turbines. *Iranian Journal of Science and Technology, Transactions of Mechanical Engineering*, *45*, 473–485. https://doi.org/10.1007/s40997-020-00410-4

Fujisawa, N. (1992). On the torque mechanism of Savonius rotors. *Journal of Wind Engineering and Industrial Aerodynamics*, *40*, 277-292. https://doi.org/10.1016/0167-6105(92)90380-S

Guerri, O., Hamdouni A., & Sakout, A. (2008). Numerical simulation of the flow around oscillating wind turbine airfoils. Part 1: Forced oscillating airfoil. *International Journal of Multiphysics, 2*(4). https://doi.org/10.1260/1750-9548.2.4.367

Guerri, O., Sakout A., & Bouhadef, K. (2007) Simulation of the fluid flow around a rotating vertical axis wind turbine, *Wind Engineering*, *31*(3). https://doi.org/10.1260/030952407781998819

Hesami, A., Nikseresht, A. H., & Mohamed, M. H. (2022). Feasibility study of twin-rotor Savonius wind turbine incorporated with a wind-lens. *Ocean Enginnering*, *247*, 110654**.** https://doi.org/10.1016/j.oceaneng.2022.110654

Im, H., & Kim, B. (2022). Power performance analysis based on Savonius wind turbine blade design and layout optimization through rotor wake flow analysis. *Energies*, *15*, 9500. https://doi.org / 10.3390 / en15249500

Johannes, S. S. (1929). *Rotor adapted to be driven by wind or flowing water*. U. S. p. N. 1697574.

Kacprzak, K., Liskeiwicz, G., & Sobczakb, K. (2013). Numerical investigation of conventional and modified Savonius wind turbines. *Renewable Energy, 60*, 578–585. https://doi.org/10.1016/j.renene.2013.06.009

Kamoji, M. A., Kedare, S. B., & Prabhu, S. V. (2008). Experimental investigations on the effect of overlap ratio and blade edge conditions on the performance of conventional savonius rotor. *Wind Engineering*, *32* (2), 163–178. https://doi.org/10.1260/030952408784815826

Menter, F. R. (1993). Zonal Two equation k-ω turbulence models for aerodynamic flows. *AIAA Paper*, 93-2906. https://doi.org/10.2514/6.1993-2906

Meziane, M., Essadiqi, E., Faqir, M., & Ghanameh, M. F. (2019). CFD study of unsteady flow through Savonius wind turbine clusters. *International Journal of Renewable Energy Research*, *9*(2), 657–666. https://doi.org/10.20508/ijrer.v9i2.8973.g7635

Mohamed, M. H., Janiga, G., Pap, E., & Thévenin, D. (2011). Optimal blade shape of a modified Savonius turbine using an obstacle shielding the returning blade. *Energy Conversion and Management*, *52*(1), 236–242. https://doi.org/10.1016/j.enconman.2010.06.070

Patel, U. K., Alom, N., & Saha, U. K. (2023). Aerodynamic analysis of a 2-stage elliptical-bladed Savonius wind rotor: Numerical simulation and experimental validation. *International Journal of Green Energy*. https://doi.org/10.1080 / 15435075.2023 – 2194975

Rahai, H. R. (2005). *Development of optimum design configuration and performance for vertical axis wind turbine.* Feasibility Analysis and Final EISG Report; California Energy Commission: Sacramento, CA, USA.

Roy, S., & Saha, U. K. (2013). Review on the numerical investigation into the design and development of Savonius wind rotors. *Renewable Sustainable Energy Review*, *2*, 73–83. https://doi.org/10.1016/j.rser.2013.03.060

Saha, U. K., Thotla, S., & Maity, D. (2008). Optimum design configuration of Savonius rotor through wind tunnel experiments. *Journal of Wind Engineering and Industrial Aerodynamics*, *96*(8), 1359–1375. https://doi.org/10.1016/j.jweia.2008.03.005

Sevasegaram, S. (1978). An experimental investigation of a class of resistance-type direction independent wind turbines. *Energy*, *3*(1), 23–30. https://doi.org/10.1016/0360-5442(78)90053-1

Shaheen, M., El-Sayed, M., & Abdallah, S. (2015). Numerical study of two bucket Savonius wind turbine cluster. *Journal of Wind Engineering and Industrial Aerodynamics, 137*, 78–89. https://doi.org/10.1016/j.jweia.2014.12.002.

Shashikumar, C. M., Honnasiddaiah, R., Hindasageri, V., & Madav, V. (2021). Experimental and numerical investigation of novel V-shaped rotor for hydropower utilisations. *Ocean Engineering, 224*, 108689. https://doi.org/10.1016/j.oceaneng.2021.108689.

Sun, X., Luo, D., Huang, D., & Wu, G. (2021). Numerical study on coupling effects among multiple Savonius turbines. *Journal of Renewable and Sustainable Energy, 4*, 053107. https://doi.org/10.1063/1.4754438

Tata, M., Smaili, A., & Masson, C. (2018). Effect of grid topology on numerical simulations of flow fields around wind turbine nacelle anemometer. *Journal of Applied Fluid Mechanics, 11*(6), 1569–1578. https://doi.org/10.29252/jafm.11.06.28925

Zhou, T., & Rempfer, D. (2013). Numerical study of detailed flow field and performance of Savonius wind turbines. *Renewable Energy*, *51*, 373–381. https://doi.org/10.1016/j.renene.2012.09.046